MJFAS MALAYSIAN JOURNAL OF FUNDAMENTAL AND APPLIED SCIENCES
PRINT ISSN: 2289-5981 | ONLINE ISSN: 2289-599X

RESEARCH ARTICLE

Ultrasound imaging characterization on tissue mimicking materials for cardiac tissue phantom: Texture analysis perspective

Nurul Shafiqa Mohd Yusof [a,b], Dyah Ekashanti Octorina Dewi [a,b,*], Ahmad 'Athif Mohd Faudzi [c], Nurulazirah Md Salih [a,b], Norzailin Abu Bakar [d], Hamzaini Abdul Hamid [d]

[a] IJN-UTM Cardiovascular Engineering Centre, Institute of Human Centered Engineering, Universiti Teknologi Malaysia, 81310, Johor, Malaysia
[b] Department of Clinical Science, Faculty of Biosciences and Medical Engineering, Universiti Teknologi Malaysia, 81310, Johor, Malaysia
[c] Department of Control and Mechatronic Engineering, Faculty of Electrical Engineering, Universiti Teknologi Malaysia, 81310, Johor, Malaysia
[d] Department of Radiology, Universiti Kebangsaan Malaysia Medical Center, 56000, Cheras, Malaysia

* Corresponding author: dyah@utm.my

Article history
Received 15 October 2017
Accepted 6 December 2017

Graphical abstract

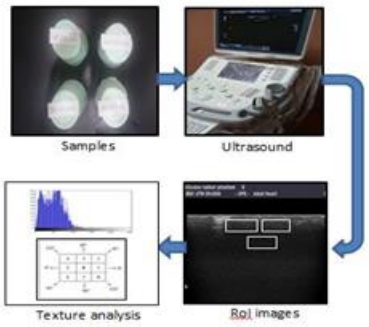

Abstract

Cardiac tissue phantom is a synthetic physical model to mimic the characteristics of actual cardiac tissues. Tissue Mimicking Materials have been widely used as materials for medical imaging phantom. In cardiac ultrasound imaging, phantoms have been used for system verification, simulation and training for cardiovascular radiography. In this study, we aimed to characterize the structure of cardiac tissue phantom by performing ultrasound imaging and texture analysis. The phantom samples were developed by mixing Silicone Rubber with Calcium Carbonate in different percentages. Ultrasound imaging with various Dynamic Range settings (30, 60, and 90 dB) was used to scan the phantom samples. First-, Second-, and Higher order Statistical Texture Analyses were used to quantify structural features of the phantom samples. As comparison, one ultrasound image of adult heart was also characterized. The results show that the addition of Calcium Carbonate affected the imaging structure of the phantom samples. Textural comparison with the ultrasound image of adult heart also confirmed that phantom with Silicon Rubber and 8% of Calcium carbonate had closest texture features.

Keywords: Cardiac tissue phantom, tissue mimicking materials, ultrasound imaging, texture analysis, silicone rubber

INTRODUCTION

Cardiac imaging phantoms, both physical and digital, have been widely used to model the heart organ in medical imaging procedures for in-vitro and in-vivo settings (Rostylav et al. 2009). Although the generic models have been commercially available, customization and optimization are still needed to obtain the best imaging technique to be implemented in the clinical settings. Specifically, problems in image quality variation in different machines and patient variabilities have been found to complicate the learning process for imaging operators (Guppy-Coles et al. 2015; Soslow et al. 2000). For this reason, customized phantom design and fabrication are needed to gain better precision with a known structure. In this regard, physical phantom may provide a more realistic experience to the ultrasound operators, as they have actual physical and haptic representation.

Ultrasound (US) imaging, as one of medical imaging modalities to capture and analyze the heart, is capable of visualizing any cardiac abnormalities from its structural, morphological, and motion features. This modality is clinically preferred to support diagnosis and guide surgeries because of its non-invasive, real-time, and cost effective advantages (Louise et al 2010). Additionally, with quantitative features in the US machine, any cardiac measurement and analysis can be quantified more precisely. However, due to dependency to operator's skill, the effectiveness of the US imaging can only be guaranteed if it is conducted by trained person.

In imaging perspectives, cardiac tissue structures may indicate certain pathological status of the heart by quantitatively characterizing their textural patterns. One of the techniques in this field is using texture analysis. Since this is quite a classical method, a large number of texture analysis techniques have been studied for many applications. Studies of (Molinari et al. 2015; Gao et al. 2014) have utilized texture analysis techniques for characterizing tissue images. For its simplicity of implementation, ease of interpretation, and suitability for natural patterns, statistical texture analysis techniques are the most commonly used techniques in biomedical fields (Depeursinge et al. 2014). It can be represented by the way that the graylevels are distributed over the pixels and interconnected among pixels in the region (Haralick 1979).

Tissue Mimicking Materials (TMMs) are important materials that can be modelled in anatomical, mechanical and internal structures for characterization, calibration, and learning tools of medical imaging system (Culjat et al. 2010; Lamouche et al. 2012). TMMs are usually made from the materials of chemically synthesized polymer (CSP) (e.g. silicone and urethane) or biopolymer materials (e.g. agar and gelatine). However, CSPs have most popular materials, as they have large varieties of mechanical properties and can preserve in much longer time. On the other hand, biopolymers may provide a good likely properties of soft tissue (Culjat et al. 2010; Chen & Shih 2013).

In this research, a new improved cardiac tissue phantom for US imaging using Silicon Rubber (SR) material has been developed. Use of Calcium Carbonate ($CaCO_3$) has been also investigated as additive to obtain improved attenuation in the US image. The objective of this study is to characterize the structure of cardiac tissue phantom by performing US imaging and texture analysis, as well as to define the best composition and texture feature for cardiac tissue phantom.

METHODOLOGY

The experimental design of this study was comprised of four main steps; material selection, fabrication, US imaging, and texture analysis. Fig. 1 illustrates the flow of the experimental design in this study.

Material selection

Among the TMMs, CSP materials were preferred for the cardiac tissue phantom development. One of the CSPs, SR, with its durability, stability, could sustain much longer for at least 10 years and give satisfying stiffness variations from kPa to MPa (Lamouche et al. 2012). Furthermore, the mechanical properties of SR-based materials were representative for cardiac tissue physical models (Culjat et al. 2010; Zell et al. 2007; Maitz 2015). Therefore, we had chosen SR as the basis material for the cardiac tissue phantom in this work.

However, as one of the main imaging issues in SR is attenuation weakness that might affect image quality and interpretation of the cardiac tissue (Culjat et al. 2010), additive materials could be added to improve the performance. In this way, these materials might act as modifiers to the SR, so that the TMMs imaging characteristics could be actually matched to the biological cardiac tissue, even to many other soft tissues. Thus, these modifiers were ideal for tissue simulators. The modifier could be sodium chloride to manipulate the electrical properties, propylene glycol (PPG) to manipulate the thermal properties, or deoinized water to hydrate the materials (Chen & Shih 2013). Not only imaging properties, the addition of ion had also been known to affect the elasticity properties of the main materials (Chen & Shih 2013). However, different modifier materials had different purpose of applications, depending on the needs of testing.

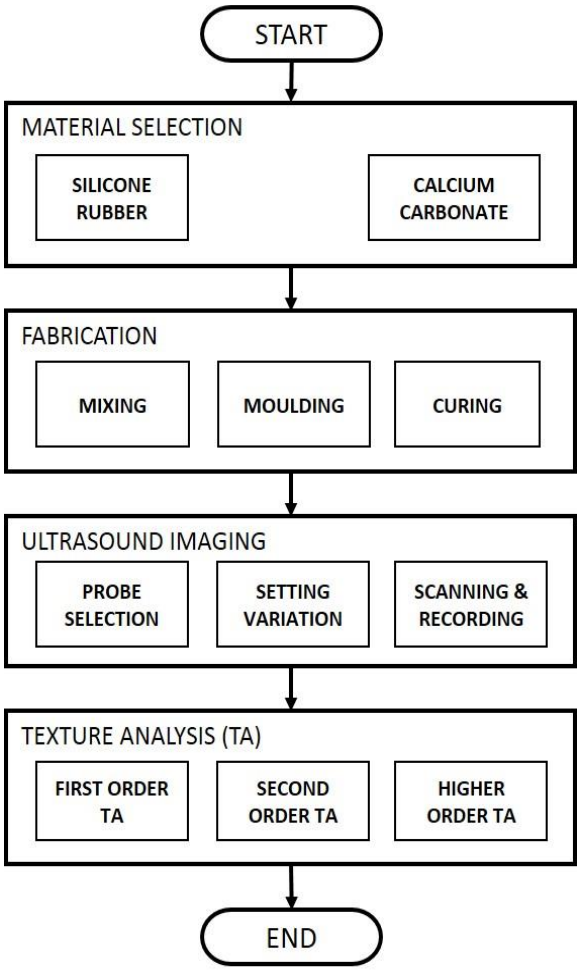

Fig. 1 Experimental design of cardiac tissue phantom fabrication and characterization.

In compensating the imaging attenuation drawback of SR, the use of additive modifiers had been suggested to improve the attenuation properties under imaging observation, thus increasing the image quality, especially contrast. $CaCO_3$ was the most common additive that had been used to increase the material density and create specific internal structures of the material. Addition of additive modifiers to the some base materials had also shown to alter their mechanical properties. The polymer-additive interaction led to the formation at the internal structure and deformation characteristics (Shirotani 1988; Meyers et al. 2011).

In this study, we used SR (Multifilla^{TM}, Malaysia) as basis material and its catalyst that built the cardiac tissue phantom, and $CaCO_3$ (Qrec, New Zealand) as the additive material. Both materials were combined through the fabrication process.

Fabrication

The fabrication process determined the composition between the basis material (SR) and additive material ($CaCO_3$). In this study, we prepared 4 types of TMM samples (SR1, SR2, SR3 and SR4) with different percentages of $CaCO_3$. Each different percentages were weighed and added up into the SR material. Table 1 describes the composition variation in the cardiac tissue phantom. The mixture of samples were stirred in few seconds, then its catalyst for about 4% by total weight was added after SR and $CaCO_3$ were well-mixed before poured into the molds. The moulds of samples were shaped in cylindrical sized-container with the dimension of 5cm in diameter and 9cm in height. Then, the samples were cured for solidification in room temperature for 24 hours.

Table 1 Compositions of cardiac tissue phantom samples.

Samples	Composition
SR1	SR + 0% $CaCO_3$
SR2	SR + 4% $CaCO_3$
SR3	SR + 8% $CaCO_3$
SR4	SR + 12% $CaCO_3$

Ultrasound Procedures and Equipment

US imaging was performed to capture the tissue structure images in the samples, as shown in Fig. 2. We conducted the experiment using US Toshiba Aplio MX (Toshiba Medical System, Tokyo, Japan) with linear probe of 8MHz, Adult Heart mode, Tissue Harmonic (TH) ON, and various modes of Dynamic Range (DR) on 30dB, 60dB, and 90dB. All system setting parameters were kept constant throughout the study of each sample. The pictures in TIFF format were transferred to a computer. The US image results were randomly trimmed into 3 Region of Interests (RoIs) with size of 70 × 30 pixels, as shown in Fig. 3, for texture analysis purposes.

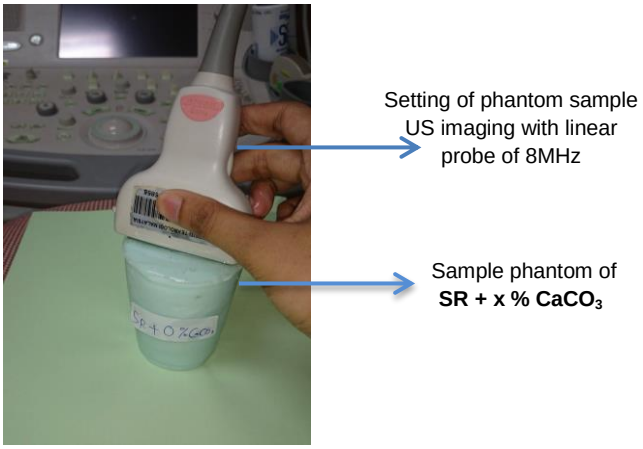

Fig. 2 Experimental setup of US imaging of cardiac tissue phantom sample.

As comparison with the cardiac tissue phantom samples, one adult heart US image sample was obtained from the image library of an open source echocardiography teaching and training website (http://www.echocardiographer.org/TTE.html). From the information, the image was acquired using Transthoracic echocardiography (TTE) technique with Parasternal Long Axis View (Dynamic Range of 65dB) in JPEG format. The adult US image in Fig. 4 was localized in certain tissue region. Similar to those of cardiac tissue phantom, the localized tissue region was trimmed into 3 Region of Interests (RoIs) with 70 × 30 pixels size for texture analysis, as shown in Fig. 5.

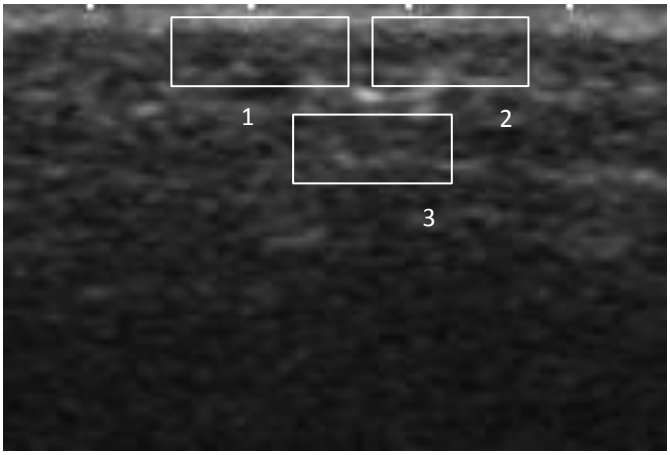

Fig. 3 Three random RoIs cropped from US images of the cardiac tissue phantom.

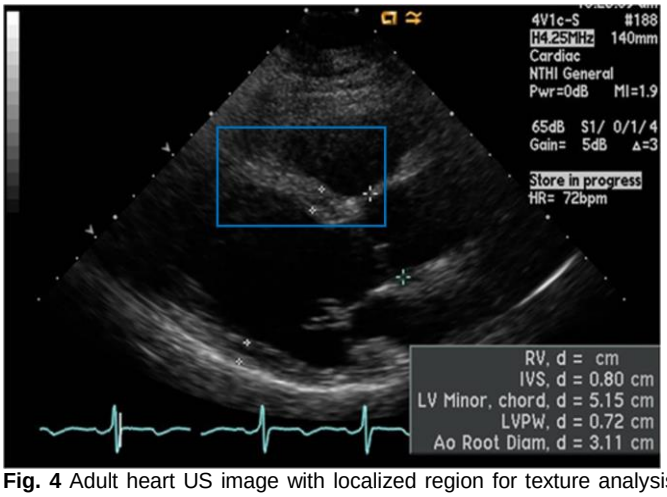

Fig. 4 Adult heart US image with localized region for texture analysis. (taken from http://www.echocardiographer.org/TTE.html)

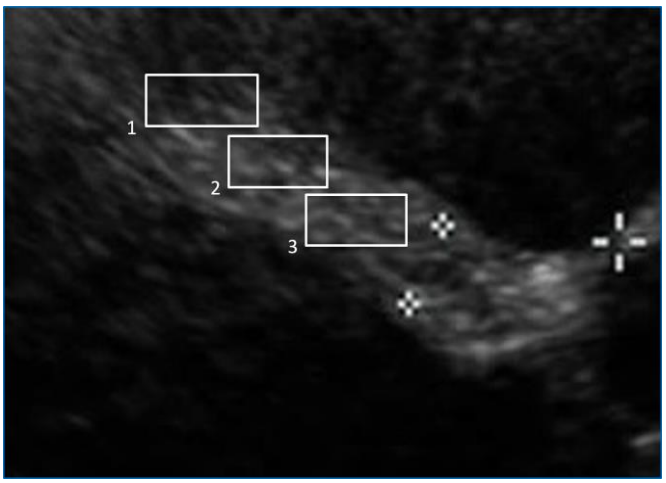

Fig. 5 The localized region with three RoIs cropped in the adult heart US image.

Texture analysis

Texture analyses (First-order, Second-order and Higher-order Statistics) were used to extract textural features. All texture analysis techniques were computed using Matlab R2013a.

First-order texture analysis is based on histogram statistical characteristics calculated from every image value (Selvarajah & Kodituwakku 2011; Nailon 2012). For any image, grey-levels are in the range of $0 \le i \le N_g - 1$, where N_g is the total number of distinct grey-levels. If $N(i)$ is the number of pixels with intensity I, M is the total number of pixels in an image, it follows that the histogram is given by,

$$P(i) = \frac{N(i)}{M} \quad (1)$$

Table 2 presents mathematical description of First-order features (Selvarajah & Kodituwakku 2011; Nailon 2012). In this study, 4 features of the first-order texture analysis; mean, variance, skewness, and kurtosis, were used.

The second-order texture analysis uses Gray Level Co-occurrence Matrix (GLCM), and is computed using 2 important parameters: relative distance measured in pixel numbers (d) and their angle (θ). It considers neighborhood relationships among pixels or groups of pixels (Gebejes et al. 2013)(Bharati et al. 2004). This feature selection is useful to terminate information that present in the surface texture.

Table 2 Mathematical description of first-order statistical features.

Features	Description
Mean	$m = \frac{\sum(f.x)}{\sum f}$
Variance	$\sigma^2 = \frac{\sum(x-\mu)^2}{\sum f - 1}$
Skewness	$S_k = \frac{m_3}{m_2^{3/2}}$
Kurtosis	$K_t = \frac{m_4}{m_2^2}$

Each pixel has 8 nearest-neighbours connected to it, horizontal 0°, vertical 90°, right 45° and left-diagonal 135° directions, and their 4 contrary directions, as illustrated in Fig. 6. In this study, 4 second-order texture analysis features; contrast, correlation, energy and entropy, were implemented. Table 3 gives mathematical description of these features.

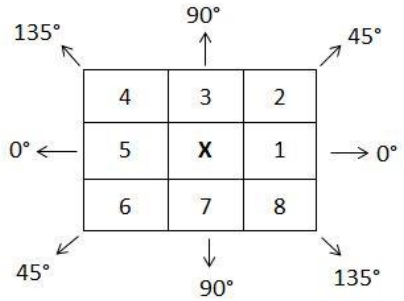

(a)

Orrientation angle (θ)	Offset
0°	[0 d]
45°	[-d d]
90°	[-d 0]
135°	[-d -d]

(b)

Fig. 6 Second-order texture analysis with (a) 8 nearest-neighbourhood scheme for obtaining co-occurrence matrix, and (b) list of orientation angle and offset.

Table 3 Mathematical description of second-order statistical features.

Features	Description
Contrast	$I_{cont} = \frac{\left(\sum_i \sum_j (ij)(GLCM_{ij})^2 - \mu_x \mu_y\right)}{(\sigma_x \sigma_y)}$
Correlation	$I_{corr} = \frac{\left(\sum_i \sum_j (ij)(GLCM_{ij})^2 - \mu_x \mu_y\right)}{(\sigma_x \sigma_y)}$
Energy	$I_{engy} = \sum_i \sum_j \left(GLCM_{ij}\right)^2$
Entropy	$I_{entp} = \sum_i \sum_j GLCM_{ij}\left(log_2 GLCM_{ij}\right)$

Table 4 Mathematical description of higher-order statistical features.

Features	Description
GLN	$GLN = \frac{1}{N_r} \sum_i \left(\sum_j P_g(i,j) \right)^2$
RLN	$RLN = \frac{1}{N_r} \sum_i \left(\sum_j P_r(i,j) \right)^2$
LGRE	$LGRE = \frac{1}{N_r} \sum_i \sum_j P_g \frac{(i,j)}{i^2}$
HGRE	$HGRE = \frac{1}{N_r} \sum_i \sum_j P_r(i,j) \cdot i^2$

Higher order texture analysis is based on the information extracted on the run of a particular grey-level, or grey-level range, in a particular direction, usually horizontal and vertical directions of the pixels. Pixel *R(i,j)* contains the number of pixels with run length *j* and intensity *i* in a given direction (Selvarajah & Kodituwakku 2011; Nailon 2012). The run length matrix (RLM) has a number of rows equal to the number of graylevels in the image and a number of columns equal to the maximum length of the run length. The studies of (Molinari et al. 2015; Mary 1975) confirmed that long graylevel runs might exist more frequently compared to the fine texture, which generally contained short runs. Table 4 shows mathematical description of these features. The texture features that we used were GLN, (Gray Level Nonuniformity), RLN, (Run Length Nonuniformity), LGRE, (Low Gray Level Run Emphasis), and HGRE, (High Gray Level Run emphasis) (Chappard et al. 2005). N_r is the total number of runs, P_g is the maximum number of grey-levels and P_r is the number of different run length in the matrix.

RESULTS AND DISCUSSION

The US imaging experiments resulted in US images of the cardiac tissur phantom samples of SR + x % $CaCO_3$, where x was 0%, 4%, 8% and 12%. A set of RoIs from each US image were taken. As comparison, RoIs from the adult heart US image were also produced. The examples of the US RoI images are given in Fig. 7. From these US RoI images, we can depict 4 analyses, the effect of DR value to the structure and shades, the use of SR as TMM in cardiac tissue phantom, the role of additive material ($CaCO_3$) in enhancing the structural visibility of the SR, as well as the comparison of the US RoI images of TMM with those of adult heart US RoI images in texture analysis point of view.

As DR determines the displayed intensity range, its effect in the US image quality is prominent in textures generated by small reflections. In the context of understanding the effect of DR value to the structure and shades, it can be visually seen that the texture image varies with different setting of DR. This is due to the fact that adjustments in DR value affect the contrast, causing alteration in structural visibility and shading effect of the image. As a result, the structures in all RoIs of DR 30 dB setting visually have highest contrast, followed by those of DR 60dB, adult heart, and DR 90dB. Conversely, the shades increase with the increase of DR. Based on these results, we can infer that similar tissue may have different structural visibility and shading effect when scanned in different DR setting. Variation in DR settings seems to give a straight forward analysis, as the low DR setting may result in better image than in higher DR setting. Therefore, as US imaging has high operator depencency, determining the optimum US imaging setting play an essential role in obtaining the best image result that represents the actual characteristics.

In analyzing the use of SR as the base material in TMM for cardiac tissue phantom in US imaging, we can refer to the results of the SR + 0% $CaCO_3$ as in Fig. 7. It can be infered that the RoIs of SR + 0% $CaCO_3$ US image have been affected by DR. Furthermore, from the structural patterns of reflected signals in the RoI images, it can also be seen that US signal has capability to penetrate properly through the cardiac tissue phantom made from the SR material in certain degree of thickness. This may indicate that the SR material is visually prospective to be a good TMM for cardiac tissue phantom in US imaging. However, its performance in certifying the biological tissue mimicking properties needs to be further investigated.

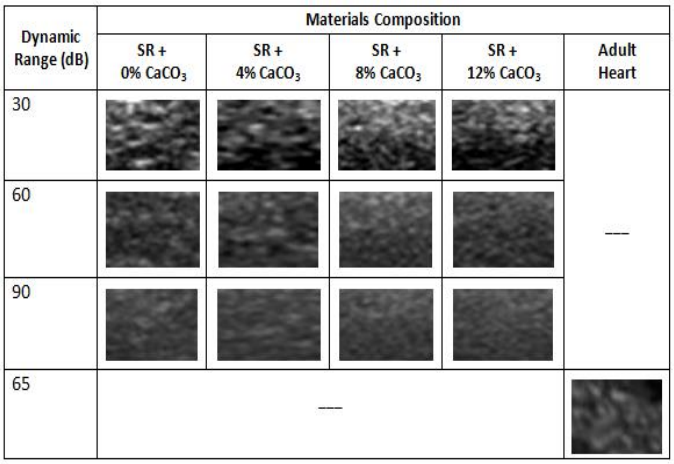

Fig. 7 RoIs of US images samples of SR + x% $CaCO_3$ with various settings of DR in 30, 60 and 90 dB as well as RoI of US image of adult heart at DR 65dB.

As $CaCO_3$ may play role as attenuation additive in the US image, combination in SR + x % $CaCO_3$ has been expected to increase the acoustic attenuation under US imaging. The RoI US images with the proportion of $CaCO_3$ in 0%, 4%, 8% and 12% in Fig. 7 show that the structural patterns of reflected signals in the RoI images increase with the increasing procentage of $CaCO_3$ in SR. This can be visually revealed from increasing internal density and reflection structure in the RoI US images. Additionally, besides density, $CaCO_3$ also tends to result in higher texture strength. Yet, acoustic attenuation measurement needs to be done to exactly confirm the role of $CaCO_3$.

In structural characterization perspective, texture analysis is one of powerful techniques in computer vision to quantify and extract the textural features based on the given image in certain RoI. These textural features may provide textural patterns based on its graylevel frequency distribution (first-order statistical analysis), point-to-point pixel connectivity (second-order statistical analysis), and run length composition (higher-order statistical analysis), that reveal important characteristics of the image. These features may also become comparison parameters in the TTM development.

For the first-order statistical analysis, Fig. 8 presents the histogram representation of RoI US image of the cardiac tissue phantom with various composition of $CaCO_3$ in DR 60dB (Fig. 8 a-d) and that of the adult heart (Fig. 8 e). From these histogram plots, we can infer that the contrast slightly decreases with the increase of $CaCO_3$. Although the contrast has the tendency to decrease, the addition of $CaCO_3$ seems to provide more graylevel details in the image. This can be clearly observed from the stretched graylevel frequency patterns in the histogram that cause slight decreased contrast in the image.

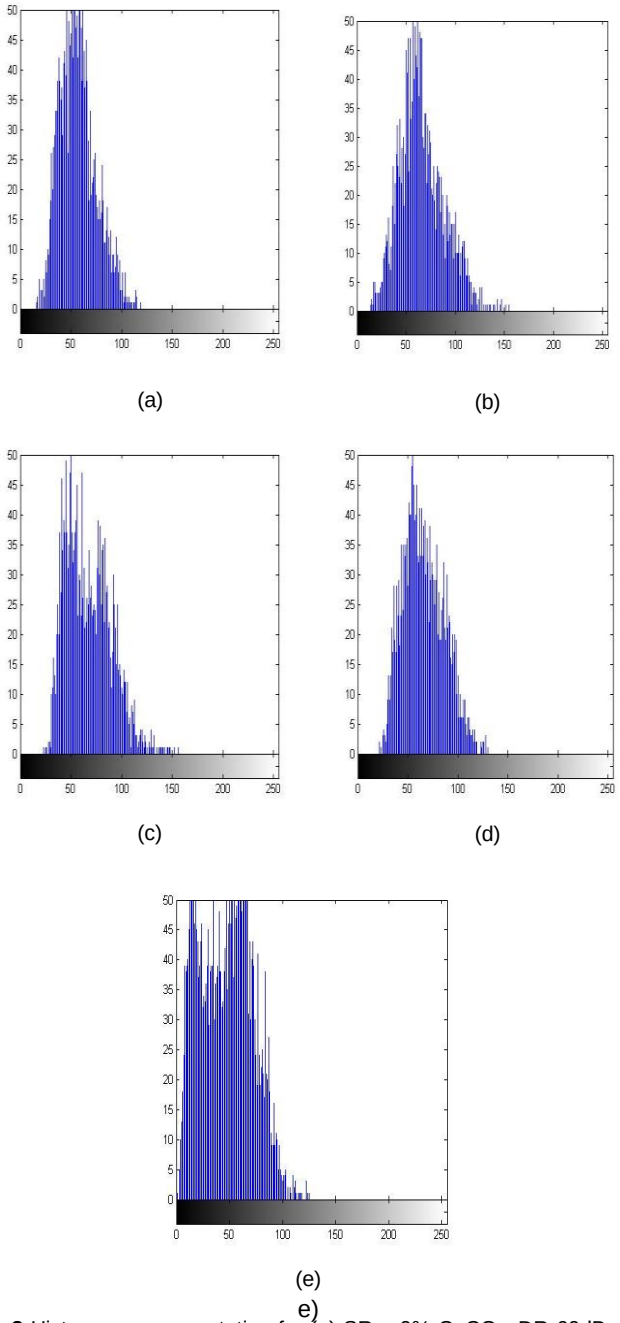

Fig. 8 Histogram representation for (a) SR + 0% $CaCO_3$, DR 60dB, (b) SR + 4% $CaCO_3$, 60 dB, (c) SR +8% $CaCO_3$,60 dB, (d) SR + 12% $CaCO_3$, 60dB, and (e) Adult heart at DR of 65 dB.

From the histogram plots in Fig. 8, textural features in the first-order statistical analysis, such as mean, variance, skewness, and kurtosis, can be generated. In this regard, investigation of textural changes in alteration of DR can also performed more thoroughly. From the first-order texture quantification, it can be seen that all textural features of the cardiac tissue phantom samples has generally similar trends along with the increment of DR. Fig. 9 shows the first-order texture features for mean (a) and kurtosis (b). For the mean feature, all phantom samples in DR 60dB and DR 90dB has almost similar values for around 60. Mean and kurtosis features seem to give better results in comparison to the other features. Compared to the adult heart features from the mean and kurtosis features, the features are approximately almost similar to the composition of SR + 8% $CaCO_3$ values at DR 60 dB. The other useful features that affect the surface texture can also be worked out from different DR settings. Thus, other than mean and kurtosis, variance and skewness features also provide textural information, but it does not seem to show good performance as good texture descriptor.

For the relationship between the first-order texture features with DR settings, DR 30dB in SR + 8% $CaCO_3$ has the highest mean values as in Fig. 9(a). On the other hand, SR + 4% $CaCO_3$ has the lowest mean values. Conversely, for variance feature in DR 30dB, SR + 8% $CaCO_3$ has the lowest variance values and SR + 4% $CaCO_3$ has the highest variance values. Also, all phantom samples has decreasing trend with the increasing percentage of $CaCO_3$ in skewness feature. For SR + 0% $CaCO_3$, the highest skewness value is obtained along with the increment of DR, while SR + 12% $CaCO_3$ has the lowest value along with the increment of DR. Kurtosis has similar trend with the skewness feature. As in Fig. 9(b), kurtosis feature decreases with the increasing of $CaCO_3$ percentage. SR + 0% $CaCO_3$ has the highest kurtosis value along with the increment of DR, while SR + 8% $CaCO_3$ and SR + 12% $CaCO_3$ have the highest values for all DR settings. These results show that addition of $CaCO_3$ in SR affect textural properties. As the materials were from CSP categories, the texture feature results have shown slight inconsistences.

The second-order statistical analysis results that represent contrast and energy features with distance d = 1 are displayed in Fig. 10. It reveals that the full set of second-order texture features, contrast, correlation, energy, and entropy generally have similar characteristics. They decrease along with the increment of DR. Decreasing values from 30dB to 90dB occurr in contrast, correlation, and entropy features, while energy feature has increasing values. In contrast feature, SR + 0% $CaCO_3$ has highest value along with the increment of DR. While SR + 4% $CaCO_3$ and SR + 12% $CaCO_3$ have the lowest contrast features for all DR. In correlation feature, DR 30 dB has the highest value with increment of $CaCO_3$. In energy feature, SR + 4% $CaCO_3$ in DR 90dB has the highest value with the increment of $CaCO_3$. DR 30dB has the lowest value of energy feature with the increment of $CaCO_3$. Entropy feature shows slightly similar characteristics with 4 to 6 entropy features for all $CaCO_3$ composition and DR settings. In the second-order texture features, only contrast and energy features have given the best results. Contrast feature values in SR + 8% $CaCO_3$ tend to have similar structures to the adult heart features with soft texture based on the low contrast. While energy feature, it was measured based on the local homogeneity of the texture in the range energy of [0,1]. Therefore, the lower the energy value, the lower the homogeneity feature of the texture. The GLCM actually indicates the selection of the best composition from a group of pixels at the same distance and direction as the texture features. This is applicable in the adult heart US image.

For the second-order statistical analysis as displayed in Fig. 11, it shows that what visually seems to be a texture element strongly corresponds to the contrast and energy features according to the distance values that represent periodicity in the texture. The distance behaviour of texture features in the TMMs has close similarities to that of the adult heart texture features. This suggests that it is possible to pick any distance in any sample of composition, because all seems to be closely comparable to the adult heart features. In this regard, we chose distance of 1.

Similarly, we characterized the materials using the other approach of statistical textural features, higher-order statistical analysis. The higher-order statistical analysis, as shown in Fig. 12, confirm that GLN, RLN, LGRE, and HGRE in general have similar characteristics with the increment of DR. As shown in Fig. 11, GLN and LGRE features are the representatives of higher order features that have influence in suggesting good texture descriptors. However, the other two features, RLN and HGRE do not exhibit significance compared to the GLN and LGRE features. In the GLN feature, the values have similar characteristics in the range of 400 to 600 in all DR. While, RLN feature has the value range of 2000 to 3000 in all DR. Also, HGRE has the value range of 400 to 600. However, in LGRE feature, image in 60dB and 90dB has similar value range of 40 to 60, while in 30dB, the lowest value range is 30 to 50. As we compare to the adult heart image, it seems that GLN feature of SR + 8% $CaCO_3$ in 60dB has approximately equal feature values. On the other hand, it seems that larger difference in LGRE between the adult heart US image and cardiac tissue phantom result in dissimilarity.

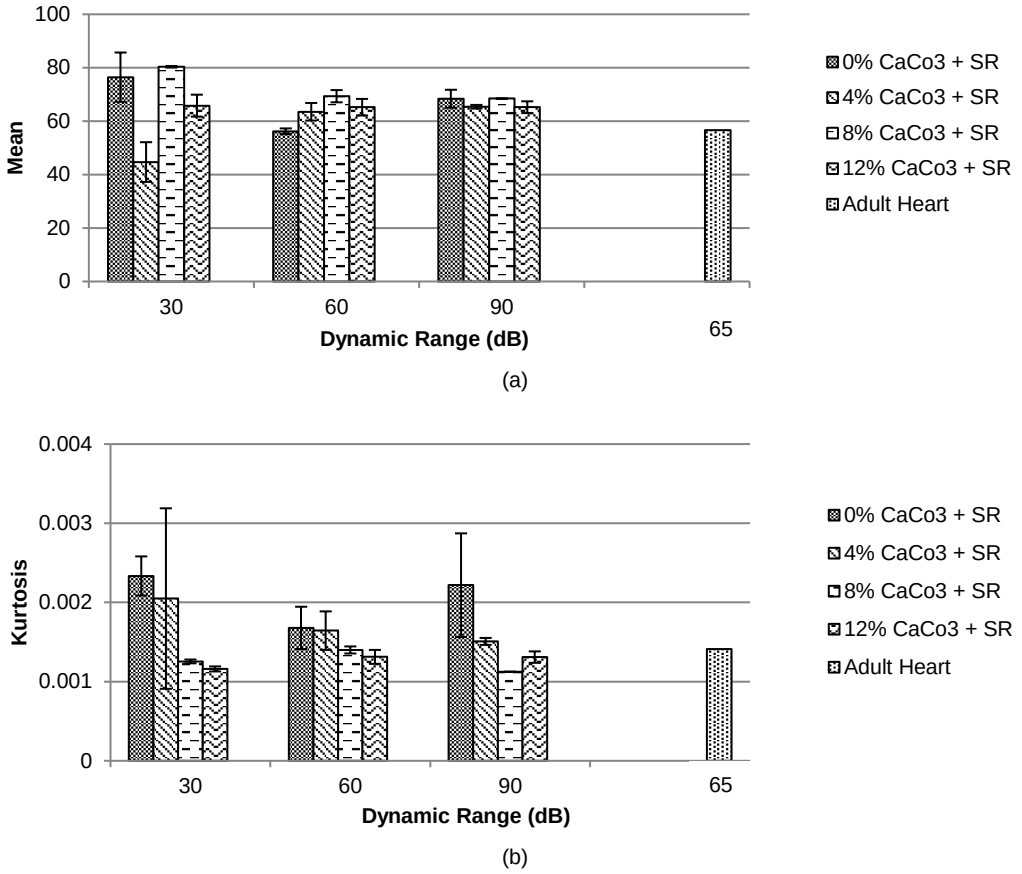

Fig. 9 First-order statistical feature plots of phantom US image for (a) Mean and (b) Kurtosis

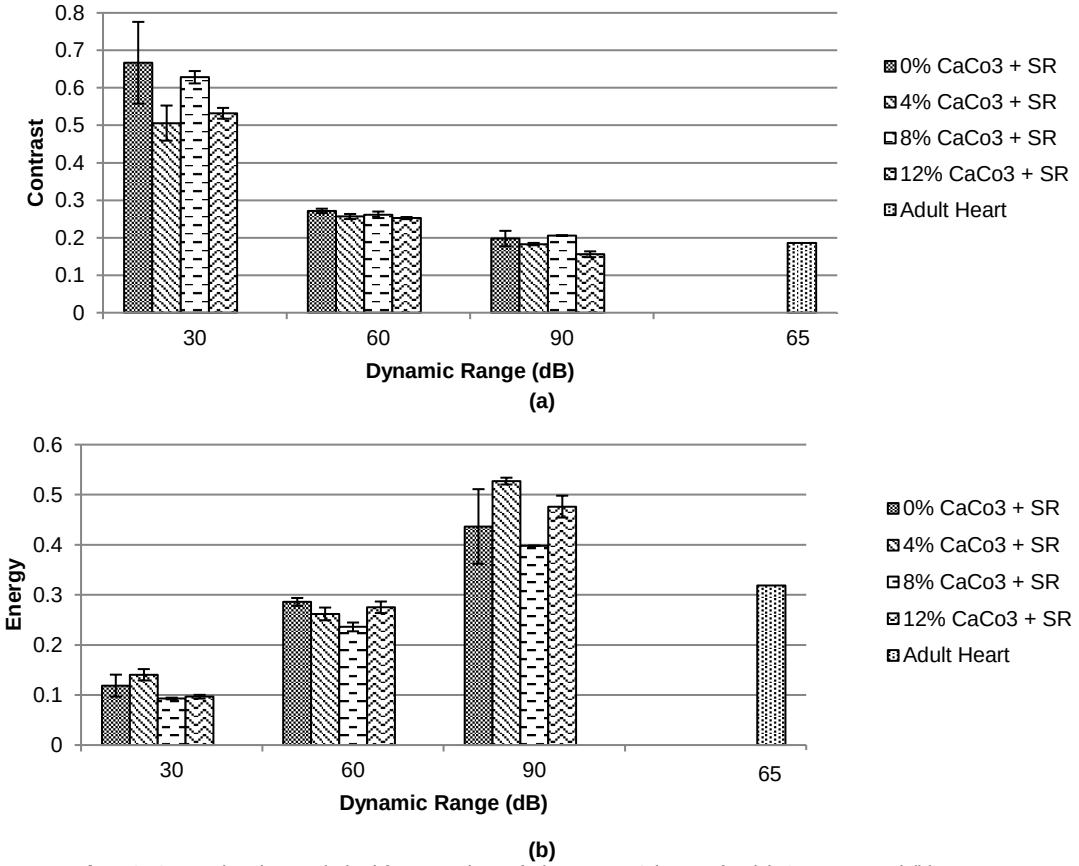

Fig. 10 Second-order statistical feature plots of phantom US image for (a) Contrast and (b) Energy

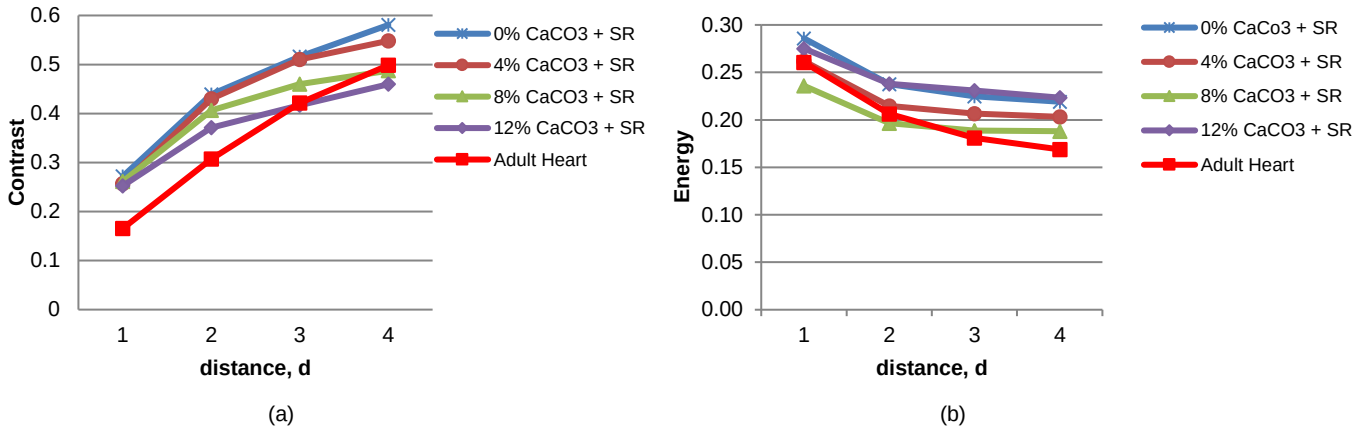

Fig. 11 Second-Order Texture Analysis Features and Distance representation for SR + 0% $CaCO_3$, DR 60dB, SR + 4% $CaCO_3$, 60 dB, SR +8% $CaCO_3$,60 dB, SR + 12% $CaCO_3$, 60 dB, and Adult heart at DR of 65dB with (a) Contrast and (b) Energy features.

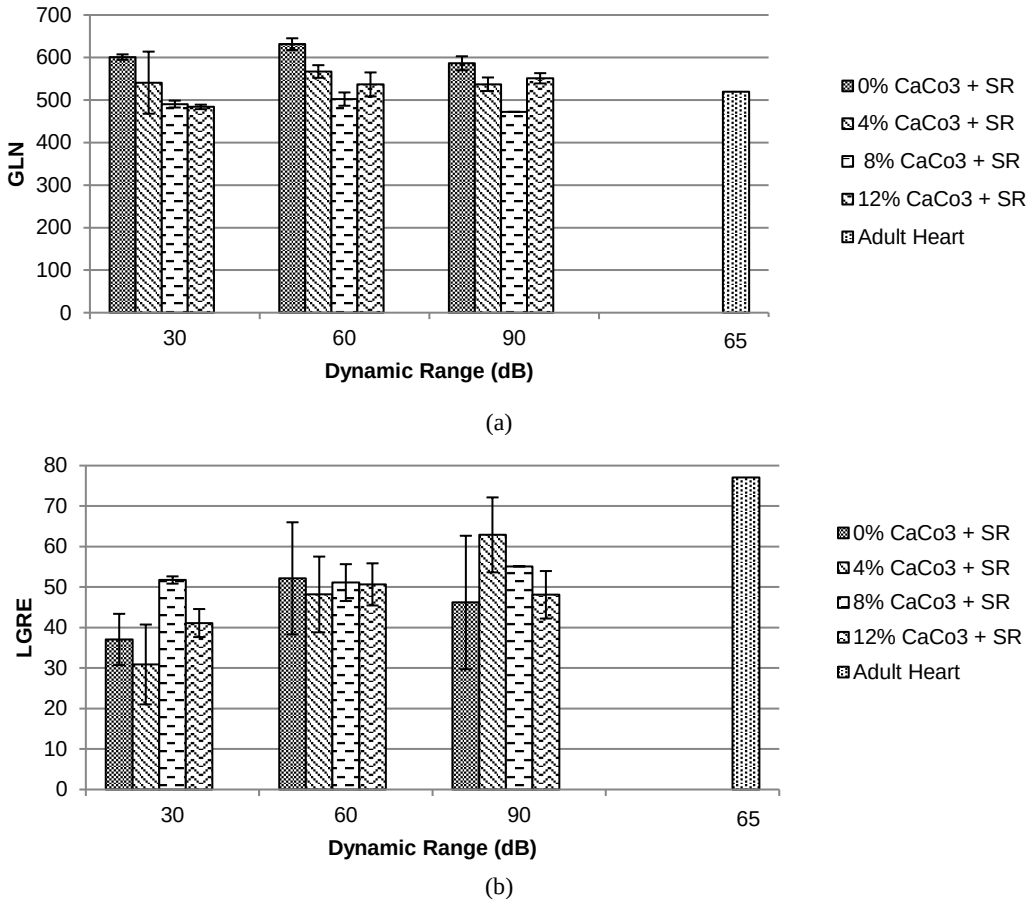

Fig. 12 Higher-order statistical features plots of phantom US image for (a) GLN and (b) LGRE features

Besides confirming promising results, our study on cardiac tissue phantoms also has some limitations. Further study with more adult heart US images with various clinical cases is required to perform better experimental design and compare with the best estimation. In this work, we have focused on texture features of the TMMs at the same thickness only. In reality, real heart may exhibit different thickness by different persons and different abnormalities. In the present study, we also found that various texture descriptors are helpful to analyze these correlations. In spite of these results, the textural features still have limitations in its clinial use because of setting dependecies to the US imaging, where each type of US imaging has its own specific settings. In this paper, we have demonstrated the importance of using $CaCO_3$ in the cardiac tissue phantom construction. Certain experiments have led to a good classification score that enables for correctly characterizing the features. However, because of the complexity and limitation of silicone polymers-based tissue substitutes, it is necessary to test with many parameters and equipment. In this way, characterization of the composition and structure can be made more precisely to mimic the human cardiac tissues. Besides, the results show that texture characteristics strongly depend on the surface of the samples materials from the US imaging. Thus, accurate result is highly dependent on the preparation, composition interaction that form the end results of the samples, and the operator. Additionally, the design of the phantoms can be affected by other factors, such as tissue thickness, composition of soft and other tissues, and temperature. In the present study, these factors are only limited by using cylindrical samples prepared with various composition of $CaCO_3$ without temperature changes.

CONCLUSION

The study has verified that cardiac tissue phantom for US imaging can be developed using SR. Variations in $CaCO_3$ percentage as additive material also provide various attenuation patterns. US imaging settings, especially DR, also play role in defining specific textural features of phantom samples. From the experiment, we found that mean, kurtosis, contrast, energy and GLN are the most influencing features in mimicking the adult heart tissue under US imaging. To conclude, there exist three important issues about the parameters in texture features in the present study: those describing the material composition, those related to the DR settings, and comparison of adult heart feature values.

ACKNOWLEDGEMENT

The authors would like to thank UTM and MOHE under FRGS Grant R.J130000.7845.4F764 and AUNSEED Net Grant R.J130000.7323.4B187. The authors also would like to thank Dr. Atif Qasim and Dr. Amresh Raina for the credit to use the adult heart echocardiography image from the echocardiography training website, http://www.echocardiographer.org/TTE.html.

REFERENCES

Bharati M. H., Liu J. J. & MacGregor J. F., 2004. Image texture analysis: methods and comparisons. *Chemometrics and Intelligent Laboratory Systems*, 72(1), pp.57–71.

Chappard D., Guggenbuhl P., Legrand E., Basle M. F., Audran M., 2005. Texture analysis of X-ray radiographs is correlated with bone histomorphometry. *Journal of Bone and Mineral Metabolism*, 23(1), pp.24–29.

Chen R. & Shih A. J., 2013. Multi-modality gellan gum-based tissue-mimicking phantom with targeted mechanical, electrical, and thermal properties. *Physics in Medicine and Biology*, 58(16), pp.5511–5525.

Culjat M.O., Goldenberg D., Tewari P., Singh R. S., 2010. A review of tissue substitutes for ultrasound imaging. *Ultrasound in Medicine and Biology*, 36(6), pp.861–873.

Depeursinge A., Foncubierta-Rodrique A., Van De Ville D., Muller H., 2014. Three-dimensional solid texture analysis in biomedical imaging: Review and opportunities. *Medical Image Analysis*, 18(1), pp.176–196.

Gao S., Peng Y., Guo H., Liu W., Gao T., Xu Y., Tang X., 2014. Texture analysis and classification of ultrasound liver images. *Bio-medical materials and engineering*, 24(1), pp.1209–1216.

Gebejes A., Huertas R., 2013. Texture characterization based on grey-level co-occurrence matrix. *Conference of Informatics and Management Sciences*, 25-29 March 2013, Slovakia, EDIS - Publishing Institution of the University of Zilina, pp.375–378.

Guppy-Coles K., Prasad S., Hillier S., Smith K., Lo A., Sippel J., Biswas N., Dahiya A., Atherton J., 2015. Accuracy of an operator-independent left ventricular ejection fraction quantification algorithm (Auto LVQ) with three-dimensional echocardiography: A comparison with cardiac magnetic resonance imaging. *Heart, Lung and Circulation*, 24(3), pp.S319–S320.

Haralick, R. M., 1979. Statistical and structural approaches to texture. *Proceedings of The IEEE*, 67(5), pp.786-804

Lamouche G., Kennedy B. F., Bisaillon C. E., Curatolo A., Campbell G., Pazos V., Sampson D. D., 2012. Review of tissue simulating phantoms with controllable optical, mechanical and structural properties for use in optical coherence tomography. *Biomed Optics Express*, 3(6), pp.1381–1398.

Louise M. C., Andrew J. F., Jacinta E. B., 2010. Novel tissue mimicking materials for high frequency breast ultrasound phantoms. *Ultrasound in medicine and biology*, 37(1), pp.122-135

Maitz, M. F., 2015. Applications of synthetic polymers in clinical medicine. *Biosurface and Biotribology*, 1(3), pp.161–176.

Mary M. G., 1975. Texture analysis using gray level run lengths. *Computer Graphics and Image Processing*, 4(2), pp.172–179.

Meyers M. A., Chen P., Lopez M. I., Seki Y., Lin A. Y. M., 2011. Biological materials: a materials science approach. *Journal of the Mechanical Behavior of Biomedical Materials*, 4(5), pp.626–657.

Molinari F., Caresio C., Acharya U. R., Mookiah M. R. K., Minetto M. A., 2015. Advances in quantitative muscle ultrasonography using texture analysis of ultrasound images. *Ultrasound in Medicine and Biology*, 41(9), pp.2520–2532.

Nailon W. H., 2012. Texture analysis methods for medical image characterisation, Youxin Mao, ed. *Biomedical Imaging*, InTech, DOI:10.5772/8912, pp.75–100.

Qasim A. & Raina A., Retrieved August 2017 from Echocardiographer.org website, http://www.echocardiographer.org/ index.html

Rostyslav B., Karthikayan B., Grant T G., James P O., US Patent 8 535 061 B2, 2009. Human torso phantom for imaging of heart with realistic modes of cardiac and respiratory motion.

Selvarajah S. & Kodituwakku S. R., 2011. Analysis and comparison of texture features for content based image retrieval. *International Journal of Latest Trends in Computing*, 2(1), pp.108–113.

Shirotani T., 1988. Realistic torso phantom for calibration of in-vivo transuranic-nuclide counting facilities. *Journal of Nuclear Science and Technology*, 25(11), pp.875–883.

Soslow R. A., Dannenberg A. J., Rush D., Woerner B. M., Khan K. N., Masferrer J., Koki A. T., 2000. COX-2 is expressed in human pulmonary, colonic, and mammary tumors. *Cancer*, 89(12), pp.2637–2645.

Zell K., Sperl J. I., Vogel M. W., Niessner R., Haisch C., 2007. Acoustical properties of selected tissue phantom materials for ultrasound imaging. *Physics in Medicine and Biology*, 52(20), pp.475–484.